Bioorg. Med. Chem. Lett. 39 (2021) 127848

Contents lists available at ScienceDirect

Bioorganic & Medicinal Chemistry Letters

journal homepage: www.elsevier.com/locate/bmcl

Identification of a new class of HBV capsid assembly modulator

Scott D. Kuduk [a,*], Bart Stoops [b], Richard Alexander [c], Angela M. Lam [a], Christine Espiritu [a], Robert Vogel [a], Vincent Lau [a], Klaus Klumpp [a], Osvaldo A. Flores [a], George D. Hartman [a]

[a] Novira Therapeutics, a Janssen Pharmaceuticals Company, 1400 McKean Road, Spring House, PA 19477, United States
[b] Janssen Pharmaceutica, N. V. Turnhoutseweg 30, 2340 Beerse, Belgium
[c] Janssen Research and Development, 1400 McKean Road, Spring House, PA 19477, United States

ARTICLE INFO

Keywords:
HBV
Capsid
Modulator
Urea

ABSTRACT

The HBV core protein is a druggable target of interest due to the multiple essential functions in the HBV life cycle to enable chronic HBV infection. The core protein oligomerizes to form the viral capsid, and modulation of the HBV capsid assembly has shown efficacy in clinical trials. Herein is described the identification and hit to lead SAR of a novel series of pyrazolo piperidine HBV capsid assembly modulators.

Introduction

Globally, the Hepatitis B virus (HBV) remains the most common cause of serious liver infection and disease. While highly effective vaccines are available, it has been estimated that there are >240 million people chronically infected with HBV.[1] Progression to liver cirrhosis and liver cancer, are common outcomes from chronic HBV infection, with an estimated 78,000 deaths as a direct result. Unfortunately, the currently available therapies are associated with very low cure rates (≤10% of treated chronic HBV patients show a functional cure with loss of HBV surface antigen) and require chronic treatment.[2] As such, there is significant need to identify new antivirals with novel mechanisms of action aimed at intensifying HBV suppression and production to enable improved treatment outcomes toward a cure.[3]

The HBV core protein contains 183 to 185 amino acids and has multiple essential functions in the viral life cycle ranging from viral capsid oligomerization/formation and facilitating viral replication[4] to host interactions with cccDNA and with epigenetic regulation.[5,6] In light of the fact there is no known human protein homolog, the HBV core protein represents a promising target for the development of antiviral molecules that can be selective, leading to safe and efficacious new therapies.

Capsid assembly modulators (CAMs) represent a new class of antivirals targeting the HBV core protein to disrupt the assembly process. CAMs interfere with normal assembly/viral DNA encapsidation by accelerating or misdirecting capsid assembly, thus inhibiting viral replication *in vitro*,[7,8] and *in vivo* in infected mouse models.[9,10] In addition, CAMs have been shown to block the production of both HBV DNA- and RNA-containing particles,[11,12] and the formation of cccDNA during *de novo* HBV infection,[13,14] differentiating from nucleoside analogs which only inhibit HBV DNA particle production.

The first capsid assembly modulator to enter the clinic was compound **1** (NVR 3–778, Fig. 1).[15] In phase Ib studies in naïve HBeAg positive patients, treatment with 600 mg BID of NVR 3-778 provided mean $\log_{10}$ reductions in serum HBV DNA ($\log_{10}$ IU/ml) of 1.7, showing

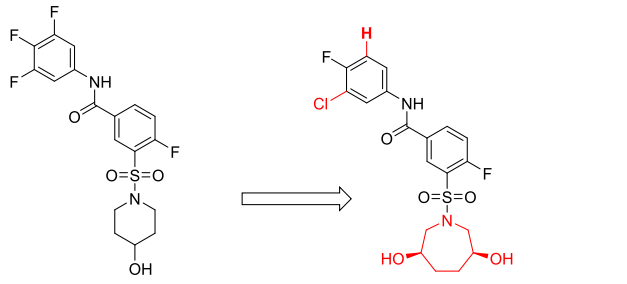

Compound 1; NVR 3-778
DNA EC_{50} = 0.47 μM
CC_{50} = 15.3 μM
~13-fold shift in 40% NHS

Compound 2
DNA EC_{50} = 0.08 μM
CC_{50} = 25.5 μM
~6.4-fold shift in 40% NHS

Fig. 1. Previous series.

* Corresponding author.
E-mail address: skuduk@its.jnj.com (S.D. Kuduk).

https://doi.org/10.1016/j.bmcl.2021.127848
Received 12 November 2020; Received in revised form 25 January 2021; Accepted 26 January 2021
Available online 18 February 2021

proof of anti-viral activity with this novel CAM mechanism of action.[16] As a first-in-class CAM, the data were promising but there were areas for improvement including modest potency and a significant shift in the presence of 40% normal human serum (NHS). Subsequent SAR work led to compound **2** that was considerably more potent and lessened the magnitude of the NHS shift.[17] However, the compounds were still in the same chemical class with modest structural distinction generated, and it was desired to identify a novel CAM chemotype. Described herein is the identification of a pyrazolopiperidine class[18] of CAM and subsequent hit to lead endeavors.

High-throughput screening of the Novira compound collection identified pyrazolopiperidine phenoxy acetamide **3** as a modestly potent CAM with an HBV DNA EC_{50} = 2.8 μM in HepG2.2.15 cells (concentration at which 50% of the HBV DNA replication is inhibited) with no overt cytotoxicity (Fig. 2). The cLogP of 4.3 indicated a quite lipophilic compound, but the pH 7 solubility was good (150 μM) and the molecular weight was reasonably low representing a good starting point. Initial SAR focused on the phenoxy acetamide region as summarized in Fig. 2. Substitution of the phenyl provided very 'flat' SAR with no meaningful potency enhancement. The linking oxygen could be replaced with CH_2, but further substitution reduced activity considerably. Similarly, the CH_2 next to the carbonyl could not tolerate any R groups, but NH or O retained activity. The C═O was essential as deletion of and replacement with a sulfonamide led to largely inactive compounds. In the context of the urea, removal of the CH_2 to generate phenyl urea **4a** led to about a 7-fold increase in cellular activity (IC_{50} = 0.39 μM) and maintained good solubility (153 μM).

Encouraged by urea **4a**, the SAR of the aryl group was explored and select compounds are shown in Table 1.[19] Placement of a chloro at the *para* (**4b**) or *ortho* (**4c**) positions lost > 3-fold potency while a *meta* analog **4d** was highly potent with an IC_{50} = 0.064 μM. Adding a fluoro at the *para* position (**4e**) had a modest improvement (IC_{50} = 0.059 μM) while 'capping' the N—H with an *N*-Me (**4f**) led to an ~ 8-fold loss of activity. Unfortunately, the 3-Cl pyridine **4g** gave a weak IC_{50} = 0.69 μM, but did return much of the solubility (136 μM) that was lost for the Cl phenyl analogs **4b-e**. Moreover, this SAR was reminiscent of the sulfonyl carboxamide series (i.e., compound **2**) where the 3-Cl-4-F phenyl was an optimal group suggesting similar overlap in the binding site.

Given the similarity of the SAR, a co-crystal structure of **4e** bound at the HBV capsid dimer-dimer interface was obtained (Fig. 3). Atomic coordinates of Y132A capsid protein complexed to compound **4e** (7K5M) have been deposited in the PDB. Hydrogen bonds are observed between the amide oxygen of **4e** and the sidechain of Trp-102, the amide nitrogen of **4e** and the sidechain of Thr-128 from the adjacent capsid dimer, and a pyrazole nitrogen of **4e** and the backbone nitrogen of Leu-140. The fluoro-chloro-phenyl group is located in a pocket defined by residues Pro-25, Asp-29, Leu-30, Trp-102, Ile105, and Ser-106 from one dimer and Val-124, Arg-127, and Thr128 of an adjacent dimer. A comparison to the crystal structure of compound **1** reported previously[20] shows a similar binding mode. The trifluoro-phenyl group in compound **1** is located in the same pocket as the chloro-phenyl group found in compound **4e**.

Next, the nature of the piperidine moiety was examined as shown in Fig. 4. Expansion from piperidine **4d** to azepane **5a** led to ~ 10-fold loss in cellular activity. Truncation from piperidine to pyrrolidine **5b** was even worse with an ~ 100-fold reduction. A two-carbon bridge in the context of the piperidine (**5c**) was also not tolerated. Lastly, replacing the piperidine with a phenyl in the form of benzamide **5d** gave an HBV DNA IC_{50} = 0.68 μM, showing the 6-membered piperidinyl urea was a vital feature for cellular activity.

Table 1
SAR of aryl urea[a].

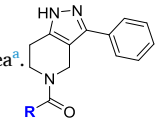

Cmpd	R	DNA EC_{50} (μM)	pH 7 Solubility (μM)
4a		0.39	153
4b	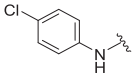	1.3	3
4c		1.6	18
4d	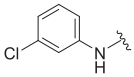	0.064	20
4e	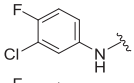	0.059	13
4f	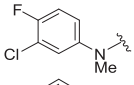	0.39	ND
4g	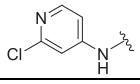	0.69	136

[a] Values represent the average of n ≥ 2 experiments. Inter-assay variability < 30%.

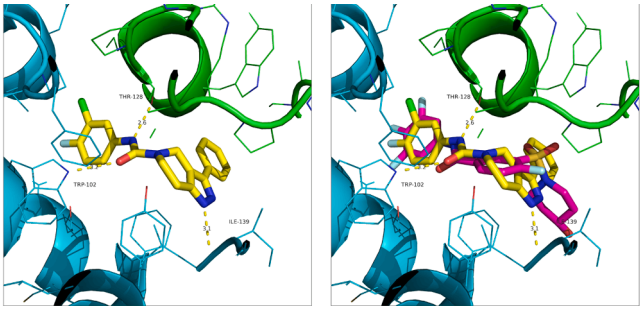

Fig. 3. Structure of the compound 4e (yellow) Y132A HBV capsid protein (cyan) complex denoting hydrogen bonds. An adjacent dimer is colored in green (left). Superposition of compound 1 (magenta, PDB code (5t2p) on the coordinates of the compound 4e HBV capsid protein complex. The relative orientation of the halogenated-phenyl ring as well as amide hydrogen bonds are conserved between the two structures (right).

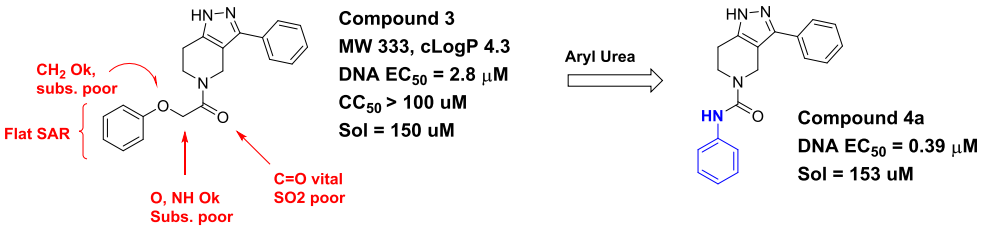

Fig. 2. Initial SAR.

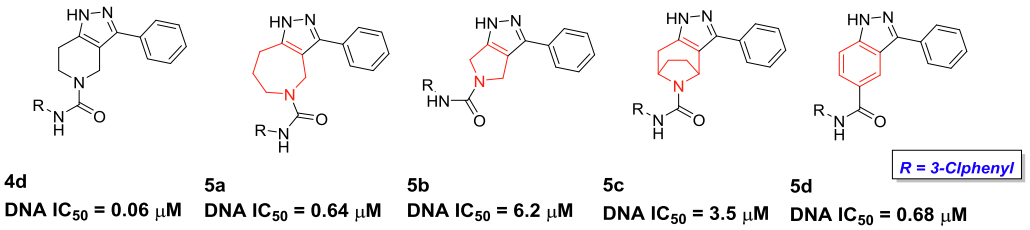

Fig. 4. Central ring SAR.

Modeling of bridged compound **5c** (not shown) indicated the binding site was too tight for the ethyl bridge, but a single methyl group at the 3- or 6-positions should be tolerated. On that basis, these compounds were prepared and profiled as shown in Fig. 5. The 6-methyl piperidines showed a notable increase in potency, with the *S* enantiomer (**6a**, IC_{50} = 0.02 μM), favored over the *R* (**6b**, IC_{50} = 0.11 μM). Thus **6a**, represents about a 3-fold improvement in potency relative to des-methyl progenitor **4d**. Moreover, The Human Microsomal Stability (HMS) Clint was dramatically reduced (15 mL/min/kg) relative to **4d** (192 mL/min/kg). In addition, the solubility was not negatively impacted by the methyl addition. The corresponding 3-methyl derivatives **6c** and **6d** were about 5–7 fold less potent.

A narrow SAR examination of the methyl group was conducted as shown in Table 2. Only compounds with the *S*-configuration are shown. The ethyl **7** was equipotent compared to methyl **6a**, with a slight decrease in solubility and microsomal stability. Vinyl **8** was the most potent amongst the group with an HBV DNA IC_{50} = 0.011 μM, but solubility and Clint continued to decrease relative to the methyl group. Lastly, the hydroxy methyl **9** lost considerable cellular potency (IC_{50} = 0.36 μM), and although solubility was dramatically improved, the Clint was the highest amongst the group. Overall, a Me group at the 6-position provided the best balance of potency, solubility, and metabolic stability.

In parallel with the examination of the piperidine SAR, replacements for the phenyl were examined. A significant number of substituted phenyl analogs adding halogen, alkyl, CN, methoxy, and hydroxymethyl substituents were examined (not shown) but the SAR proved very flat with little gains in activity. However, replacement with a range of heterocycles provided more compelling results (Table 3). Replacement of phenyl with a thiophene at the 2- (**10a**, IC_{50} = 0.016 μM) or 3-position (**10b**, IC_{50} = 0.028 μM) improved potency 2–4 fold, but significantly increased the Clint. Adding a nitrogen to **10b** to generate thiazole **10c** maintained this excellent potency profile, and also reduced the Clint. Thiazoles attached to the pyrazole at the 2- (**10d**) or 5-positions (**10e**) were less active. Isothiazole **10f** was 10-fold less potent compared to

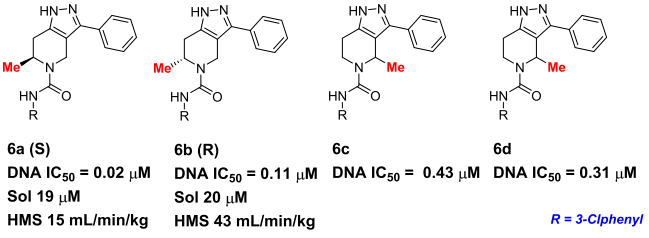

Fig. 5. Piperidine Me SAR.

Table 2

6-Position SAR[a].

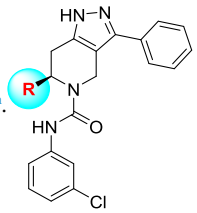

Cmpd	R	DNA EC_{50} (μM)	pH 7 Solubility (μM)	HMS Clint (ml/min/kg)
6a	Me	0.02	19	15
7	Et	0.021	9	22
8	Vinyl	0.011	4	33
9	CH_2OH	0.36	163	163

[a] Values represent the average of n ≥ 2 experiments. Inter-assay variability < 30.

Table 3

Phenyl replacements[a].

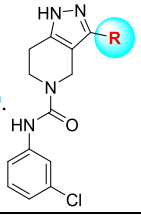

Cmpd	R	DNA EC_{50} (μM)	HMS Clint (ml/min/kg)
4a	Ph	0.064	192
10a	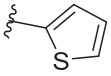	0.016	356
10b	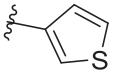	0.028	160
10c	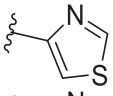	0.029	33
10d	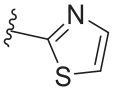	0.7	53
10e	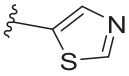	0.19	nd
10f	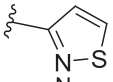	0.29	nd
10g	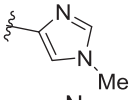	>1	nd
10h	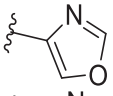	0.025	50
10i	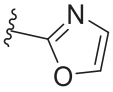	0.1	nd
10j	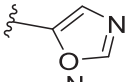	>1	nd
10k	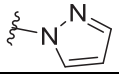	0.37	nd

[a] Values represent the average of n ≥ 2 experiments. Inter-assay variability < 30%.

thiazole **10c**, highlighting the importance of the position of the nitrogen heteroatom in the ring, Replacing the S of **10c** with an *N*-Me in the form of imidazole **10g** led to a complete ablation of activity, while insertion of an O atom at this position to oxazole **10h** led to a compound with similar activity (IC_{50} = 0.025 μM) and modestly higher Clint. The isomeric oxazoles (**10i-j**) were less active which is consistent with the corresponding thiazole compounds **10c-e**. Lastly, an *N*-linked pyrazole (**10k**) was about 6-fold less potent compared to phenyl.

The incorporation of the 6-Me with the *S*-configuration was subsequently merged with the promising phenyl replacements from Table 3. The first combination was made with highly potent thiophene **10a** to produce **11** with an HBV DNA IC_{50} = 0.007 μM (Fig. 6). While this is about a 2-fold improvement in potency, the metabolic stability was dramatically improved over des-Me **10a**, and is quite similar to the phenyl variant **6a**. In addition, methylation of the pyrazole was carried out in the context of thiophene **11**. Both isomers were prepared and methylation at the 1-position of the pyrazole (**12**) lost around 10-fold in potency, while the 2-position (**13**) lost > 25-fold highlighting the importance of the NH to H-bond with Leu140.

While it was gratifying to see the addition of the 6-Me could improve potency and the metabolic stability of the thiophene, additional SAR around the thiophene ring (not shown) did not provide any improvement in compound potency. Moreover, thiophene **11** was very lipophilic (LogD > 4.5) and replacement of the potentially bioreactive thiophene moiety was desired. Accordingly, thiazole **10c** was selected for subsequent profiling via addition of the 6-Me group.

As shown in Table 4, addition of the 6-Me to **10c** in the form of thiazole **14a** did not have a notable effect on potency, but the Clint was moderately improved relative to the des-Me variant. Moreover, the pH 7 solubility was markedly improved at 90 μM. Additional SAR on the aryl urea was then examined leveraging the learnings from Table 1. Addition of a fluorine at the 4-position of the phenyl (**14b**) led to an approximate 2-fold increase in cellular potency, but at the expense of the solubility. Interestingly, the 3-Br congener (**14c**) gave a similar profile as the Cl, but the solubility appeared to be improved despite the addition of the more lipophilic halogen. Building upon this, moving the fluorine to the 2-position and adding a nitrogen at the 4-position provided pyridine **14d**. This pyridine did have some reduced potency (IC_{50} = 0.036 μM), but had significant improvements in terms of stability and solubility. The 3-CN analog **14e** proved to be equipotent compared to the 3-halo substituents with similar stability and modestly improved solubility relative to **14c**. Lastly, the 3-Me variant (**14f**) was quite comparable to the 3-CN compound, albeit with apparent higher solubility.

The compounds were further profiled in additional selectivity assays/counter-screens and thiazole **14e** emerged as a leading compound.[21] Subsequent pharmacokinetic profiling in rat and dog was conducted (Table 5). The rat clearance was moderate, around 42% of liver blood flow with a 2.28 h half-life and 38% oral bioavailability. The liver to plasma ratio was high, ~17:1. The dog clearance was higher than rat, around 63% of liver blood flow, but with good oral bioavailability (73%) at a 2.5 mpk dose. Overall, **14e** appeared to have a good

Table 4

Urea SAR.[a]

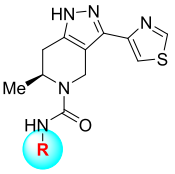

Cmpd	R	DNA EC_{50} (μM)	HMS Clint (ml/min/kg)	pH 7 Solubility (μM)
14a	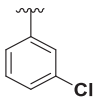	0.028	20	90
14b	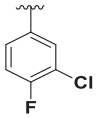	0.013	21	5
14c	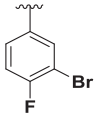	0.014	24	45
14d	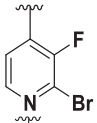	0.036	12	183
14e	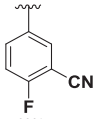	0.012	13	73
14f	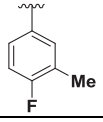	0.014	14	161

[a] Values represent the average of n ≥ 2 experiments. Inter-assay variability < 30%.

Table 5

Rat and dog Pharmacokinetics of 14e.[a,b]

Parameter	Rat PK	Dog PK
CL_p (mL/min/kg)	30.7 (42% LBF)	19.5 (63% LBF)
V_{ss} (L/kg)	2.97	3
$t_{½}$ (h)	2.28	2.17
C_{max} PO (ng/mL)	73	472
T_{max} PO (h)	6	1
$AUC_{(0\text{-inf})}$ PO (ng.h/mL)	1030	1620
L/P ($AUC_{0\text{-}24}$)	17	nd
F (%)	38	73

[a] Sprague-Dawley rats (n = 3). Oral dose 5 mg/kg, 70% PEG400 vehicle; IV dose = 1.25 mg/kg, saline vehicle.

[b] Beagle dogs (n = 3). Oral dose 2.5 mg/kg, IV dose = 1 mg/kg. Inter-animal variability was <20% for all values.

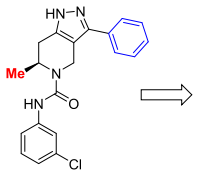

6a (S)
DNA IC_{50} = 0.02 μM
HMS 15 mL/min/kg
Sol 19 μM
H PPB: 99.3%
Log D > 4.5

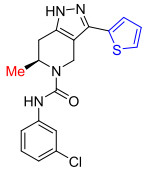

11
DNA IC_{50} = 0.007 μM
HMS 17 mL/min/kg
Sol 20 uM
H PPB: 99.5%

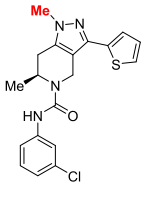

12
DNA IC_{50} = 0.077 μM
HMS 146 mL/min/kg
Sol 12 uM

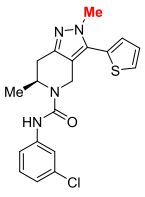

13
DNA IC_{50} = 0.2 μM

Fig. 6. Pyrazole alkylation.

balance of pH solubility (73 uM), lipophilicity (clogP 2.3), and permeability in MDR1 cells.

Lastly, the plasma shift of **14e** in the presense of 40% NHS was determined in HepG2.2.15 cells. As noted previously, NVR 3–778 has a substantial shift of ~ 13-fold. By way of comparison, thiazole **14e** had markedly reduced protein shift of ~ 3.4-fold in the presence of 40% NHS, a further improvement of this novel class of CAM.

In summary, a novel HBV CAM series has been identified via screening and H2L SAR was conducted. A urea group was found to be optimal in lieu of the initial piperidinyl amide, and a co-crystal structure with the HBV capsid indicated similar binding for the aryl urea as the earlier described sulfonyl carboxamide class of CAM. Of note, SAR on the piperidine ring led to the discovery of the addition of a 6-Me group (*S*-configuration) that not only drove potency, but had a significant improvement on metabolic stability. Further SAR of the phenyl ring extending off the pyrazole led to a number of heterocycles with improved profiles. Of note, thiazole **14e** showed excellent cellular potency compared to the sulfonyl carboxamides, a clean off-target profile, and a promising pharmacokinetic and liver exposure profile. Further optimization and exploration of this novel series of HBV CAM is ongoing to identify an optimal candidate for development.

Declaration of Competing Interest

The authors declare that they have no known competing financial interests or personal relationships that could have appeared to influence the work reported in this paper.

Acknowledgements

We thank Jan Abendroth and Christine Lukacs at Beryllium for HBV Capsid crystal growth, soaking, and structure determination of **4e**.

References

1 Cowie BC, Carville KS, MacLachlan JH. *Antivir Ther*. 2013;18:953–954.
2 Zoulim F, Lebosse F, Levrero M. *Curr Opin Virol*. 2016;18:109–116.
3 Brahmania M, Feld J, Arif A, Janssen H. *Lancet Infect Dis*. 2016;16:10–21.
4 Zlotnick A, Venkatakrishnan B, Tan Z, Lewellyn E, Turner W, Francis S. *Antiviral Res*. 2015;121:82–93.
5 Lucifora J, Xia Y, Reisinger F, et al. *Science*. 2014;343:1221–1228.
6 Guo YH, Li YN, Zhao JR, Zhang J, Yan Z. *Epigenetics*. 2011;6:720–726.
7 Deres K, Schroder CH, Paessens A, et al. *Science*. 2003;299:893–896.
8 Wang XY, Wei ZM, Wu GY, et al. *Antivir Ther*. 2012;17:793–803.
9 Weber O, Schlemmer KH, Hartmann E, et al. *Antiviral Res*. 2002;54:69–78.
10 Brezillon N, Brunelle MN, Massinet H, et al. *PLoS ONE*. 2011;6, e25096.
11 Lam A.; Ren, S.; Vogel, R.; Espiritu, C.; Kelly, M.; Lau, V.; Hartman, G.; Flores, L.; Klumpp, K. The Liver Meeting 2015 (AASLD), San Francisco, CA, 2015, Abstract 33.
12 Wang J, Shen T, Huang X, et al. *J Hepatol*. 2016;65:700–710.
13 Berke JM, Dehertogh P, Vergauwen K, et al. *Antimicrob Agents Chemother*. 2017;61 (8):e00560–17.
14 Ko C, Bester R, Zhou X, et al. *Antimicrob Agents Chemother*. 2019;64(1):e01440–19.
15 Lam AM, Espiritu C, Vogel R, et al. *Antimicrob Agents Chemother*. 2018;63:1–16.
16 Yuen M-F.; Kim D-J.; Weilert F.; Chan H.L.; Lalezari J.P.; Hwang S.G.; Nguyen T.T.; Liaw S.; Brown N.; Klumpp K.; Flores L.; Hartman G.; Gane E.J. The Liver Meeting 2015 (AASLD), San Francisco, CA, 2015, Abstract LB-10.
17 Kuduk SD, Lam AM, Espiritu C, et al. *Bioorg Med Chem Lett*. 2019;29:2405–2409.
18 Hartman, G.D., Kuduk, S.D. US 10,077, 264 B2, Sep 18, 2018.
19 Compound synthesis is described in ref 18, but the general route is exemplified as follows. Condensation of the lithium enolate of A with the thiazole acid chloride affords di-ketone B. Subsequent treatment of B with hydrazine leads to pyrazole C. Removal of the Boc group with HCl provides amine D. Lastly, condensation of D with the phenyl carbamate E generates urea 14e

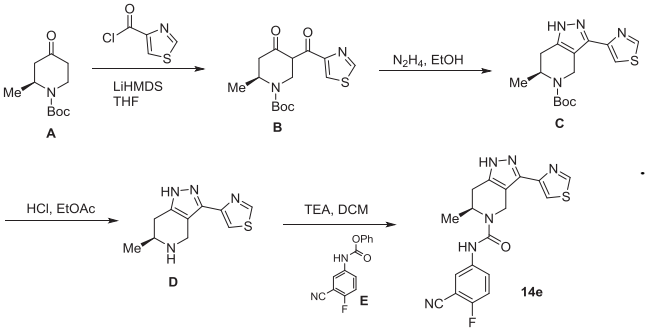

20 Zhou Z, Hu T, Zhou X, et al. *Sci Rep*. 2017;7:42374–42385.
21 The CC_{50} in HepG2.2.15 cells was > 100 μM.